(21)

H. Föll
priv. copy

phys. stat. sol. (a) 58, 393 (1980)

Subject classification: 1.4; 21.1; 21.1.1; 22.1.2

IBM Thomas J. Watson Research Center, Yorktown Heights[1]) *(a), Cornell University, Ithaca*[2]) *(b), and Institut für Physik, Max-Planck-Institut für Metallforschung, Stuttgart*[3]) *(c)*

Weak-Beam Contrast of Stacking Faults in Transmission Electron Microscopy

By

H. FÖLL (a), C. B. CARTER (b), and M. WILKENS (c)

Stacking faults (and other planar defects) imaged under weak-beam conditions can exhibit pronounced contrast changes if the sign of the diffraction vector or of the excitation error is changed. This contrast behaviour has not yet been understood. In this paper, the contrast of weak-beam images of stacking faults in silicon is studied systematically; the faults are subsequently unambiguously characterized by direct lattice imaging. Other related planar defects in silicon, stainless steel, and a copper alloy are also investigated. Extrinsic stacking faults are found to show significant contrast asymmetries while intrinsic faults did not. A simple theory is presented which taking into account the finite thickness of an extrinsic stacking fault can explain most of the observed contrast phenomena.

Stapelfelhler (und andere planare Defekte), die unter „weak-beam"-Bedingungen abgebildet werden, können ausgeprägte Änderungen im Kontrastverhalten zeigen, falls das Vorzeichen des Beugungsvektors oder des Anregungsfehlers geändert wird. Dieses Kontrastverhalten konnte bisher nicht erklärt werden. In dieser Arbeit wird der „weak-beam"-Kontrast von Stapelfehlern in Silizium systematisch untersucht; die Defekte werden anschließend durch direkte Kristallgitterabbildung eindeutig charakterisiert. Andere planare Defekte in Silizium, rostfreiem Stahl und einer Kupfer-Aluminium-Legierung werden ebenfalls untersucht. Extrinsische Stapelfehler zeigen, im Gegensatz zu intrinsischen Stapelfehlern, beträchtliche Kontrastasymmetrien. Eine einfache Theorie wird erläutert, die durch Berücksichtigung der endlichen Dicke eines extrinsischen Stapelfehlers die meisten der beobachteten Kontrasterscheinungen erklären kann.

1. Introduction

The contrast of transmission electron microscope (TEM) images of stacking faults has been studied in great detail for the case of dynamical or kinematical two-beam conditions; for reviews see [1 to 3]. Under these conditions the contrast is well understood and can be accurately simulated using standard computing methods [4]. The principal parameters entering the calculations are $\boldsymbol{R}$, the displacement vector of the fault, $\boldsymbol{g}$, the diffraction vector, s, the excitation error, d, the depth position of the fault in the foil, and T, the foil thickness. It is found that the contrast varies periodically with both d and T, giving rise to the well known stacking-fault fringes observed for a stacking fault inclined in the foil. A basic result of previous calculations is that the intensity of the fringes is independent of the sign of the product $(\boldsymbol{g} \cdot \boldsymbol{R}) \cdot s$ (apart from the change of black fringes to white ones and vice versa). However, when the weak-beam technique [5] is used it has been shown that this need not be the case for stacking faults in silicon [6, 7].

[1]) Yorktown Heights, New York 10598, USA.
[2]) Ithaka, New York 14850, USA.
[3]) Heisenbergstr. 1, D-7000 Stuttgart 80, BRD.

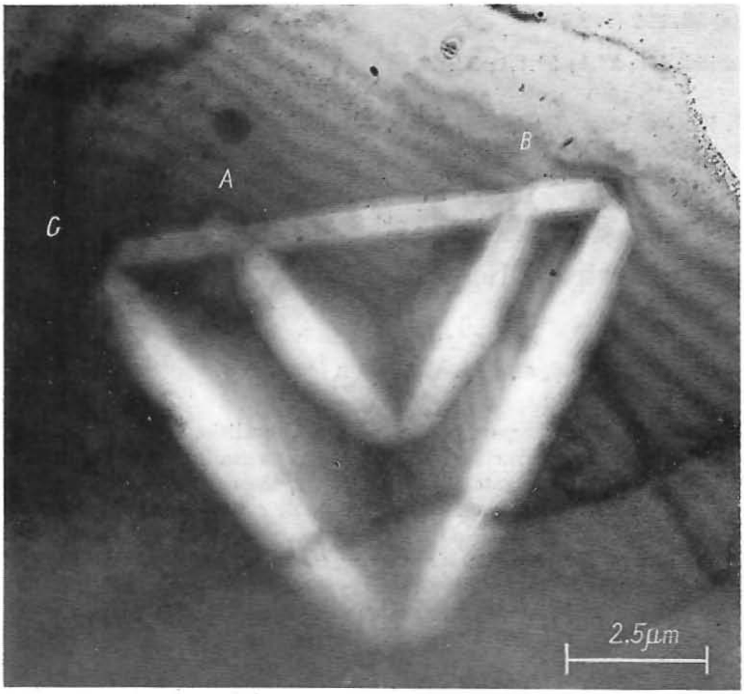

Fig. 1. Low magnification micrograph of the stacking faults in silicon which are studied in detail in Fig. 2 to 5 incl.

The experimental observation is that reversing the sign of $\boldsymbol{g}$ may change the over-all intensity of the stacking fault image from relatively high to very low [6, 7]. A similar observation has recently been made [8] for the related case of incoherent twin boundaries in both silicon and stainless steel where $\boldsymbol{R}$ then refers to the so-called rigid-body translation [9]. No explanation for the observed contrast anomaly has been offered in the literature, it therefore appeared worthwhile to re-investigate the contrast of stacking faults using weak-beam imaging conditions. Preliminary result of this study were given in [10] and the details of this investigation are the subject of this paper.

2. Extrinsic and Intrinsic Stacking Faults in Silicon

2.1 The geometry of the stacking faults investigated

The configuration of the stacking faults investigated in Si is shown in Fig. 1. The stacking faults form two truncated pyramids which appear to have one side in common. The defects occurred in the epitaxial silicon layer deposited on a {111} oriented substrate. This process frequently results in the formation of very large stacking faults [11], in this case the faults were nucleated at the end points of dislocations which moved into the substrate during the epitaxial process due to thermal stresses [11]. A short Sirtl etch treatment [12] was applied in order to identify stacking-fault rich areas; specimens of suitable size were then taken from these areas. Chemical–mechanical polishing in silica-gel was used to remove the etched layer and the specimens were then chemically thinned from the backside. The mechanical–chemical polishing however did not remove the entire etch structure and the faults thus lie in groves which outline their shape (Fig. 1). Before this investigation it had already been established that the

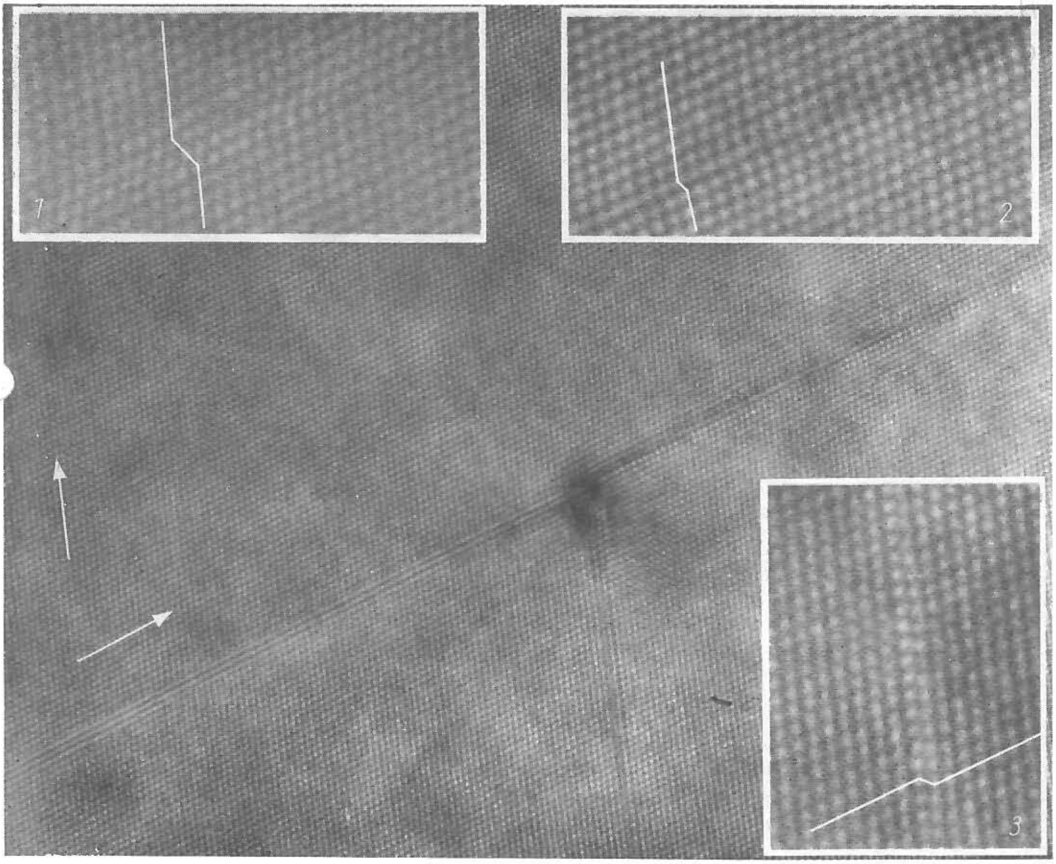

Fig. 2. Lattice image of stacking faults at area B in Fig. 1. Arrows denote traces of {111} planes

stacking faults in these samples were exclusively intrinsic in nature if they occurred as single faults or as single fault pyramids. It thus could be safely assumed that the faults forming the defect of interest were of the intrinsic type, too — except for the portion AB. This could be an intrinsic fault, an extrinsic fault, two intrinsic faults overlapping on non-adjacent planes or even a microtwin (the existence of microtwins in connection with stacking faults in epitaxial layers of Si has been demonstrated in [13]). An unambiguous distinction between these possibilities with conventional ("first-fringe") methods proved to be impossible, partly because the specimen was too thin for these methods to be applied reliably [4] and partly because a distinction between the possible defect configurations mentioned above is very difficult even under favorable conditions.

The nature of the defect was therefore ascertained by further thinning the sample using an ion-beam thinner (after the weak-beam images discussed in the next section had been taken) and then studying the area of interest using lattice imaging techniques [14, 15]. Axial illumination was used after tilting the specimen approximately 35° to the {110} pole so that the particular stacking faults could be viewed edge-on. The specimen was somewhat buckled after the ion-milling; a determination of the actual orientation within the accuracy needed for "true" structural images [14] was therefore a 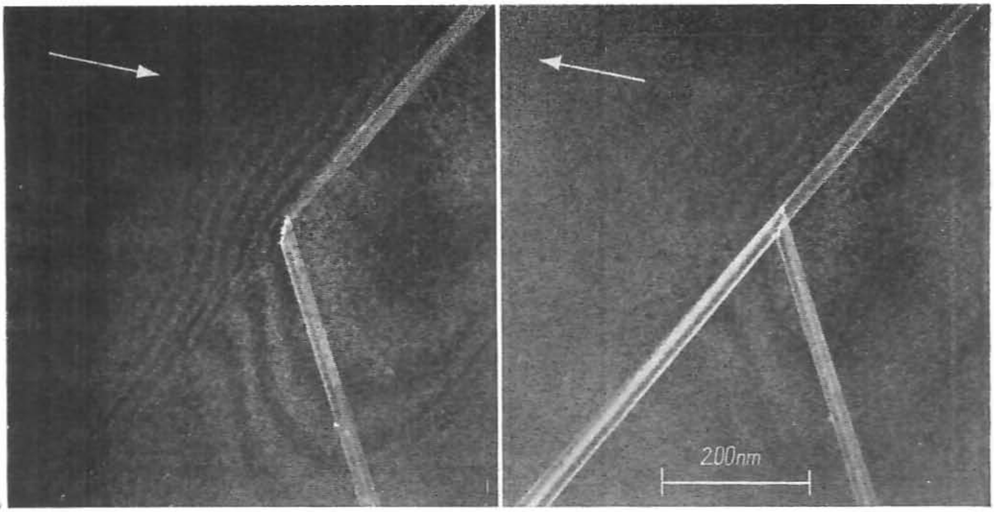 b

Fig. 3. Weak-beam image of area B. Arrows in this and in the following pictures indicate diffraction vectors. $\boldsymbol{g} = \{220\}$ in this case

not possible. In order to overcome this difficulty several sets of pictures have been taken with slightly modified imaging conditions. The microscope used was an Elmiskop 102 equipped with a tilt stage and operated at 125 keV. Fig. 2 shows the lattice image of the defect (area B); the inserts 1 and 2 are from sets of images taking under slightly different imaging conditions, insert 3 is an enlargement from this image. These images (and some twenty others not shown here) demonstrate conclusively that the defect between A and B on Fig. 1 is an extrinsic stacking fault while the other faults are intrinsic. The contrast irregularities along parts of the stacking faults in the lower magnification image of Fig. 2 are most likely due to very small tilts away from the ideal diffraction conditions and not due to the presence of impurities in the fault. This is concluded from the observation that the expected lattice image can be obtained by a small change in the diffraction conditions.

2.2 Weak-beam contrast from stacking faults in silicon

Fig. 3 shows weak-beam images of the same area shown in Fig. 2 which were obtained using $\{220\}$ reflections close to the $\{111\}$ pole. A large change in contrast on reversing $\boldsymbol{g}$ can be seen for the extrinsic stacking fault (E), while little change occurs for the intrinsic faults (I). The change in contrast of the extrinsic fault was found to be relatively insensitive to the magnitude of the excitation error s, provided this was not too small. Fig. 4 a, b shows a similar pair of weak-beam images from area A, together with an image for a larger values of s (Fig. 4f), two images using $\{111\}$ reflections and a strong-beam image. The actual diffraction conditions used are indicated in the figures. Fig. 4f does not show the intensity modulation of the stacking fault fringes visible in Fig. 3 and Fig. 4 a, b which are due to the strong coupling of $\boldsymbol{g}$ and $2\boldsymbol{g}$ [16]. Fig. 4 a, b also demonstrates that the asymmetry in the contrast is not due to particular values of the foil thickness because they show the same asymmetry as Fig. 3 a and b, although the specimen is thicker here.

From Fig. 4 c and d it appears that the contrast asymmetry does not occur, or is much less pronounced for the $\{111\}$ reflections.

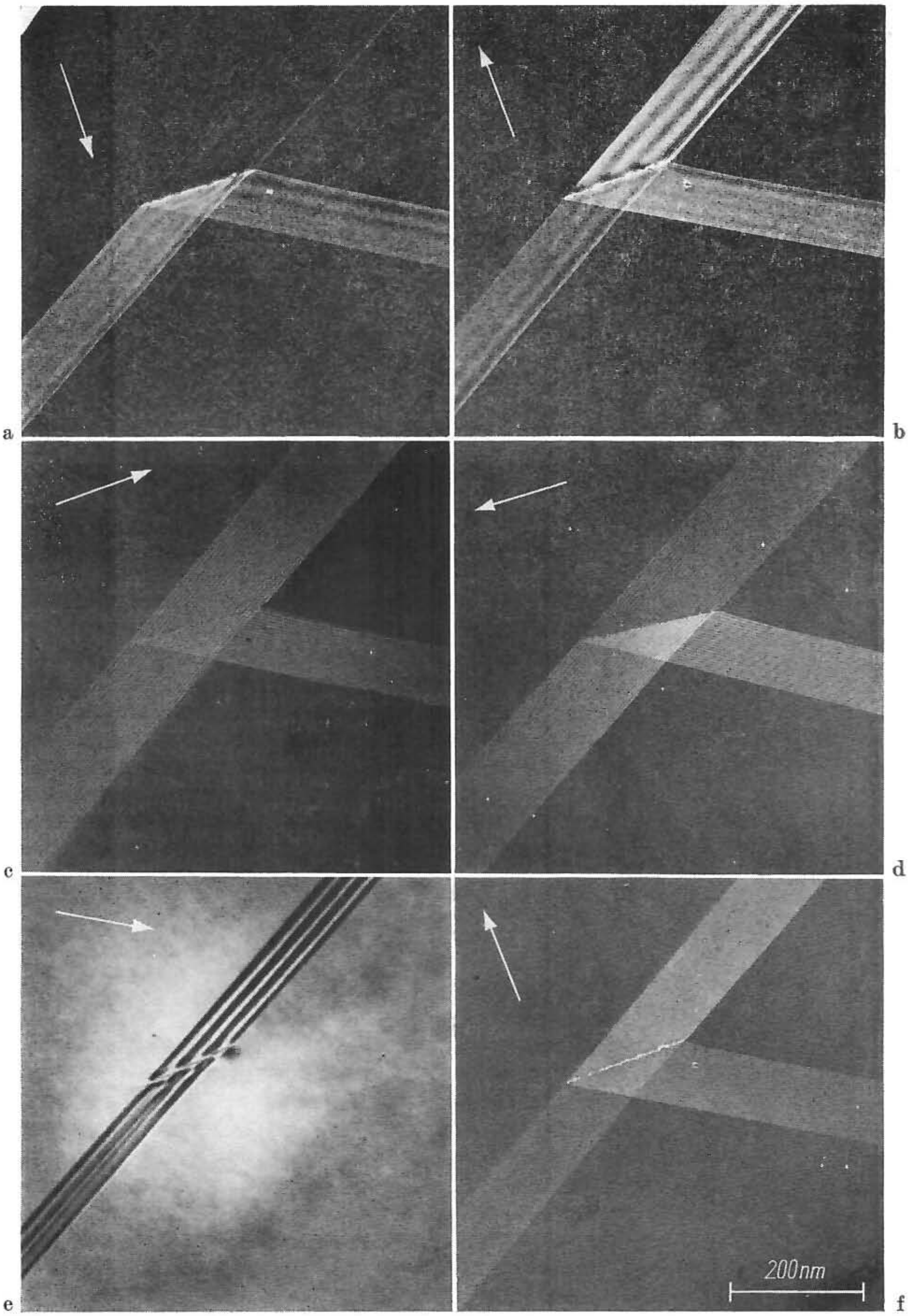

Fig. 4. Area A imaged with different diffraction vectors. a), b), e), f): $\boldsymbol{g} = \{220\}$, c), d): $\boldsymbol{g} = \{111\}$. For details see text

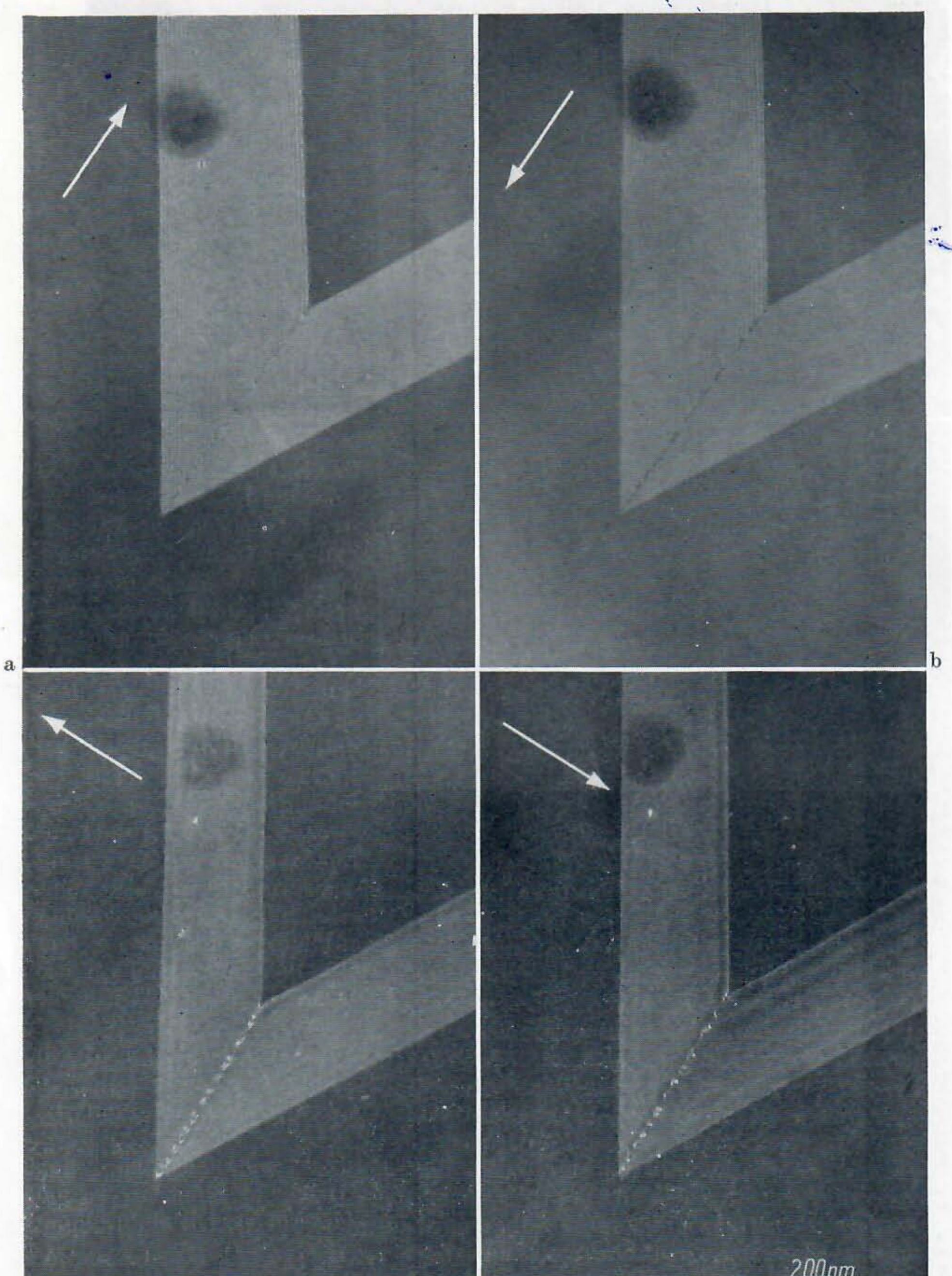

Fig. 5. Area C imaged with different diffraction vectors. a), b): $\boldsymbol{g} = \{111\}$; c), d): $\boldsymbol{g} = \{220\}$

Fig. 5 shows similar weak-beam images from area C. In this case, which is for a much thicker foil, the possibility cannot be excluded that the {111} images show some asymmetry if $\boldsymbol{g}$ is reversed (Fig. 5 a and b) even though both faults are intrinsic in nature. In contrast, the {220} reflections (Fig. 5 c and d) do not show a detectable effect. These images also show that impurity segregation has occurred along the stair-rod dislocation at the junction of the stacking faults.

Clearly, the contrast mechanism is complicated, but it can be concluded from these observations that

(i) the contrast of an extrinsic stacking fault in Si inclined with an angle of $\approx 70°$ in the foil shows a large contrast asymmetry with respect to the sign of $\boldsymbol{g}$ if weak-beam diffraction conditions and a {220} reflection is used. The contrast of an intrinsic stacking fault under identical conditions does not appreciably change;

(ii) the contrast of an extrinsic stacking fault in Si inclined with an angle of $\approx 60°$ in the foil shows no detectable contrast asymmetry with respect to the sign of $\boldsymbol{g}$ if weak-beam diffraction conditions and a {111} reflection is used. The contrast of an intrinsic fault under identical conditions may show a small asymmetry.

3. Additional Experimental Results

Contrast asymmetries from planar defects other than intrinsic and extrinsic stacking faults in silicon have also been observed. Although the geometry of these defects was not as well established as that of the stacking faults discussed above, it is worthwhile to show some examples.

Fig. 6 shows a number of overlapping stacking faults in stainless steel (the defect could be a microtwin; this is however not known with certainty) imaged using dynamical two-beam conditions and weak-beam conditions. No change in the average

a b

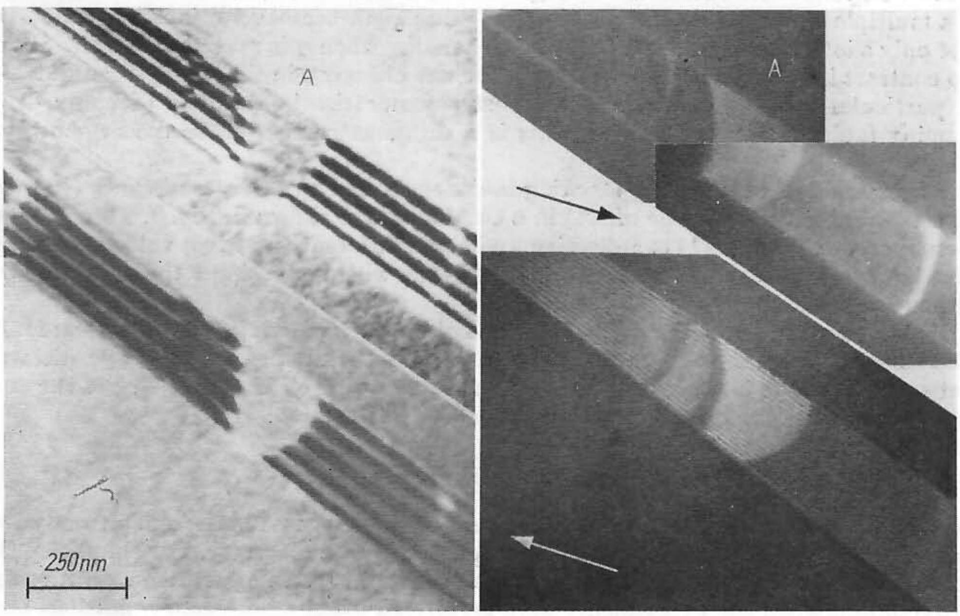

c d

Fig. 6. Overlapping stacking faults in stainless steel a), b): strong-beam images; c), d) weak-beam images; $\boldsymbol{g} = \{111\}$

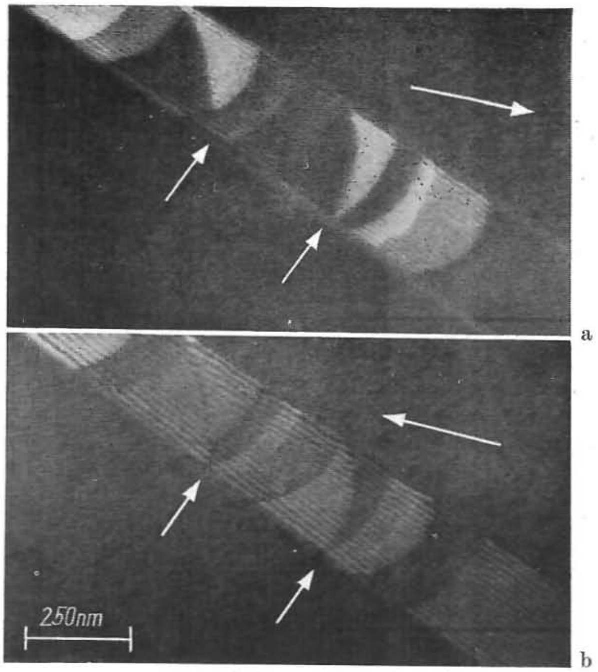

Fig. 7. Overlapping stacking faults in stainless steel. The small arrows mark identical areas; $\boldsymbol{g} = \{111\}$

contrast is observed with reversing $\boldsymbol{g}$ in the strong-beam pictures (Fig. 6 a and b); at "A" an area showing little contrast is present. This would usually be attributed to a total displacement vector $\boldsymbol{R} = \Sigma\, \boldsymbol{R}_{\text{in}} = 3n\boldsymbol{R}_{\text{in}}$ with $n = 1, 2, 3, \ldots$, so that $\alpha = 2\pi\boldsymbol{gR}$ is a multiple of 2π. The same defect imaged using weak-beam conditions (Fig. 6 c and d) not only shows strong contrast in area A (changing when $\boldsymbol{g}$ is reversed) but also shows no contrast in areas where a strong contrast was observed in the strong-beam images. A particular striking example of contrast asymmetries in the case of many overlapping faults is shown in Fig. 7, this is a different region of the defect shown in Fig. 6.

Micrographs of overlapping stacking faults separated by a larger distance (≈ 4 nm as estimated from the fringe offset) in a CuAl alloy are shown in Fig. 8. These images were recorded using a $\{111\}$ reflection and three different (positive) values of the excitation error s. It can be seen very clearly that with increasing s the contrast goes through a minimum.

Finally, Fig. 9 shows kinematical bright-field images of overlapping stacking faults in silicon. These faults have been shown not to be microtwins [17]; the distance between the faults is thought to be a few nanometers. A clear asymmetry of the contrast upon reversing $\boldsymbol{g}$ is observed in parts of the fault area.

4. Theoretical Considerations

In this section the experimental observations will be discussed both from an analytical point of view and using the concept of amplitude–phase diagrams. For simplicity the kinematical contrast theory [1 to 3] will be used; this can be justified as a first approximation when the experiments were performed using weak-beam conditions and, although particularly for the $\{220\}$ reflections dynamical effects can be strong [16], it has been found (e.g. Fig. 4) that these cannot explain the contrast asymmetry.

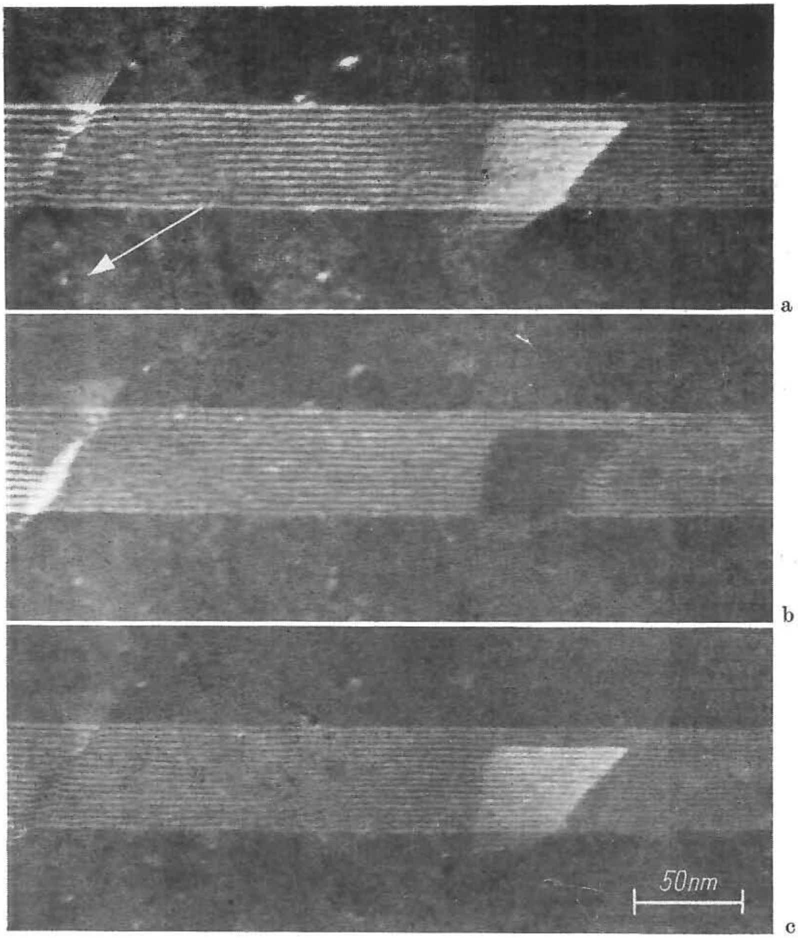

Fig. 8. Overlapping stacking faults in CuAl alloy. The magnitude of the excitation error s increases from a) to c); $\boldsymbol{g} = \{111\}$

In standard calculations [1 to 3] intrinsic or extrinsic faults are described by one translation vector $\boldsymbol{R}_{\text{int}}$ and $-\boldsymbol{R}_{\text{int}}$ (where it is assumed that $\boldsymbol{R}_{\text{ext}} = 2\boldsymbol{R}_{\text{int}} =$ lattice vector $-\boldsymbol{R}_{\text{int}}$) respectively, i.e. by *one* "cut" and a corresponding translation for either fault. This is not correct for the extrinsic fault because it consists of two *separate* translations both with magnitude $\boldsymbol{R}_{\text{int}}$ on adjacent $\{111\}$ planes. An extrinsic fault can therefore be considered to consist of two overlapping intrinsic faults on adjacent $\{111\}$ planes, Fig. 10 illustrates this. In what follows we therefore consider the general case of two overlapping intrinsic stacking faults, separated by a distance d_n (taken along the electron beam, see Fig. 10)

$$d_n = n d_{111}/\cos\theta \tag{1}$$

with d_{111} distance between adjacent $\{111\}$ planes, n number of $\{111\}$ layers between the two faults ($n = 1$ for an extrinsic fault), and θ angle of inclination of the faults with respect to the electron beam. Only if d_1 is very small compared to the effective extinction distance [1], can the extrinsic fault be described for contrast purposes by

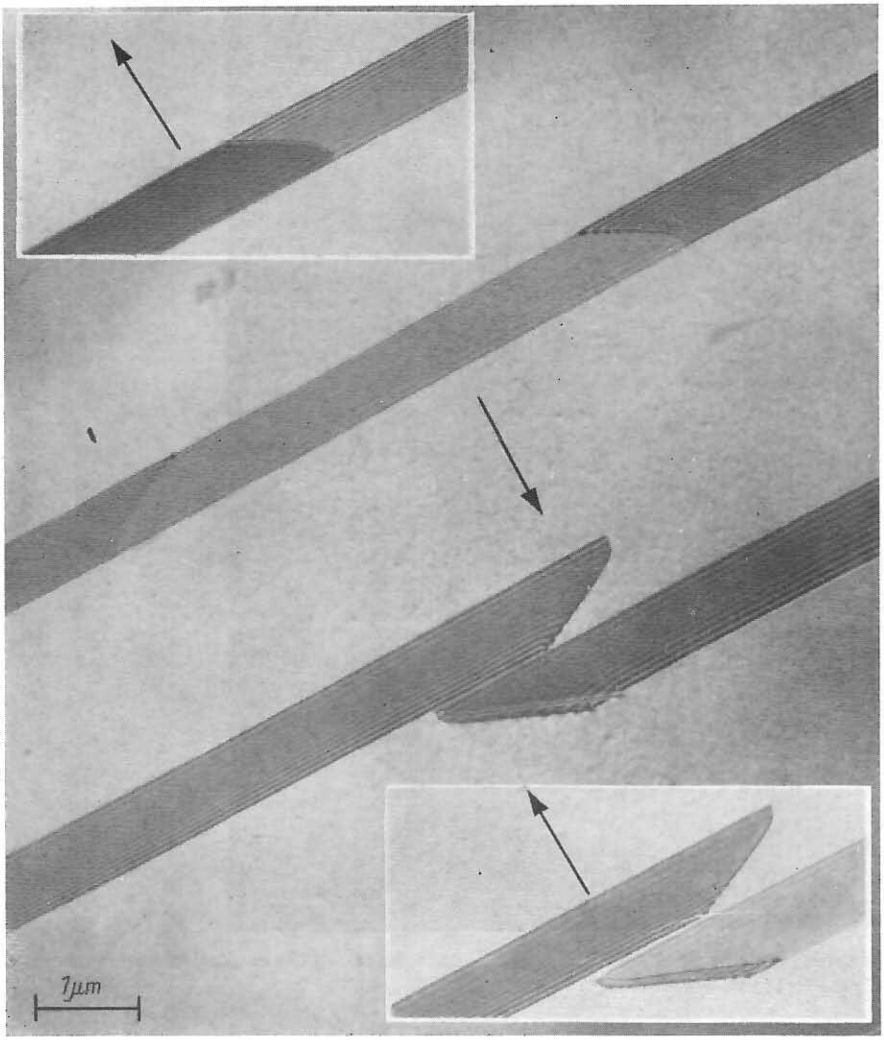

Fig. 9. Overlapping stacking faults in Si. A significant contrast change is visible upon reversing the sign of $\boldsymbol{g} = \{220\}$ as shown in the inserts

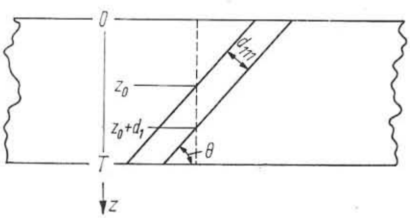

Fig. 10. Geometry of an extrinsic (or two overlapping intrinsic) stacking faults. For the column shown phase shifts occur at a depth z_0 and $z_0 + d_1$

a translation $-\boldsymbol{R}$ in one plane. This clearly is not the case for weak-beam diffraction conditions where typical values for the effective extinction distance ξ_g are $\xi_g \approx 5$ nm [5] and, for an extrinsic fault, $d_1 \approx 0.9$ nm.

With the phase shift α_{in} at an intrinsic fault

$$\alpha_{in} = 2\pi(\boldsymbol{g} \cdot \boldsymbol{R}) = \pm 120^\circ \tag{2}$$

occuring at a depth z_0 for an intrinsic fault and at a depth z_0 *and* $z_0 + d_1$ for an extrinsic fault, the amplitude of the diffracted beam is given by (apart from preexponential factors)

$$A_{in}(z_0, T) = \int_0^{z_0} \exp 2\pi isz \, dz + \exp i\alpha_{in} \int_{z_0}^{T} \exp 2\pi isz \, dz \,, \tag{3}$$

$$A_{ex}(z_0, T) = \int_0^{z_0} \exp 2\pi isz \, dz + \exp i\alpha_{in} \int_{z_0}^{z_0+d_1} \exp 2\pi isz \, dz + {} + \exp 2i\alpha_{in} \int_{z_0+d_1}^{T} \exp 2\pi isz \, dz \,. \tag{4}$$

The intensities are obtained by multiplying the amplitudes with their conjugate complexes in the usual way. The results are easily obtained, however lengthy. Since only the over-all contrast features are required the average over z_0 and T is taken and gives the average intensities $\langle I \rangle_{z,T}$

$$\langle I_{in} \rangle_{z,T} = 2 - \cos \alpha_{in} \,, \tag{5}$$

$$\langle I_{ex} \rangle_{z,T} = 3 - 2\cos \alpha_{in} + 4 \sin^2 (\alpha_{in}/2) \cos (D_1 + \alpha_{in}) \,, \tag{6}$$

where $D_1 = 2\pi s d_1$ is the magnitude of the phase shift between the faulted layers. $\alpha_{in} = 0$ gives the average background intensity (unity) and subtracting this from the above expressions, the average contrast, $\langle C \rangle$, is given by

$$\langle C_{in} \rangle = 1 - \cos \alpha_{in} = 1 - \cos (\pm 120^\circ) = 1.5 \,, \tag{7}$$

$$\langle C_{ex} \rangle = 3 + 3 \cos (D_1 + \alpha_{in}) \,. \tag{8}$$

Fig. 11 shows $\langle C_{ex} \rangle$[4]) for $\alpha_{in} = \pm 120^\circ$ as a function of D_n; the ratio of the average contrasts is also given. Clearly, the contrast of overlapping stacking faults, including extrinsic faults, is expected to show large asymmetries with respect to the sign of the phase shift α_{in}, or, more generally, with respect to the sign of $(\boldsymbol{g} \cdot \boldsymbol{R}) \cdot s$, within the framework of the kinematical two-beam theory.

It will be shown in the discussion that this theory cannot account for all the observed contrast phenomena. Nevertheless, in the belief that it provides at least the

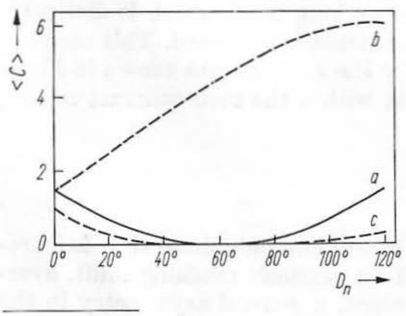

Fig. 11. The average contrast of an extrinsic stacking fault as a function of the phase shift between the two faulted planes. Curves are shown for a positive and a negative sign of the phase shift and for the ratio of the average contrast. (a) $\langle C \rangle_-$, (b) $\langle C \rangle_+$, (c) $\langle C \rangle_- / \langle C \rangle_+$

[4]) In this and in the preceding formulae the subscript "ex" stands not only for an extrinsic stacking fault but for any two overlapping faults if D_1 is replaced by the appropriate D_n.

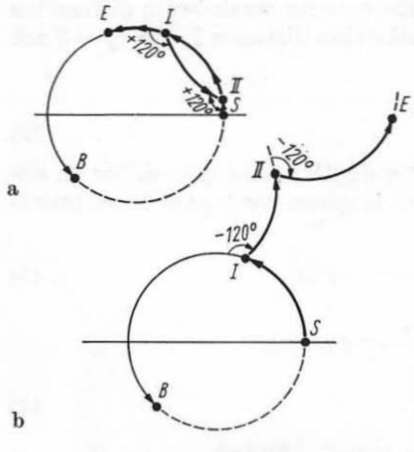

Fig. 12. Amplitude–phase diagram for zero contrast of an extrinsic stacking fault for one sign of the phase shift a) and for strong contrast for reversed phase shift b). s starting point; I, II points of first and second phase shift; E end point for fault; B end point for background contrast

correct starting point for a better understanding of the observed contrast asymmetries, the following conclusions can be drawn:

(i) If $d_n/\xi_g \gtrapprox 1/30$ (corresponding to a phase shift D_n between the two faults of $\gtrapprox 12°$), the contrast difference between two micrographs taken with $+\boldsymbol{g}$ and $-\boldsymbol{g}$, respectively, should be noticeable, (see Fig. 11) for weak-beam *and* strong-beam conditions.

(ii) *Total* contrast extinction should be observed for $D_n = 60°$ (corresponding to $d_n/\xi_g = 1/6$) and for one sign of $\boldsymbol{g}$, whereas a strong contrast should be obtained for the other sign of $\boldsymbol{g}$. This is approximately true for $45° \lessapprox D_n \lessapprox 75°$.

(iii) Contrast asymmetries similar to those discussed for two overlapping faults can be expected for more than two overlapping faults, for microtwins (more than two overlapping faults on adjacent {111} planes) and for coherent twin boundaries (an infinite number of overlapping faults on adjacent {111} planes).

(iv) If the ratio d_n/ξ_g is sufficiently large, there should always be a contrast asymmetry for two or more overlapping faults and no contrast asymmetry for planar defects with only one translation on one plane such as intrinsic stacking faults.

The perhaps surprising prediction of essentially zero contrast under certain conditions can be best illustrated with an amplitude phase diagram, drawn for $D_n = 60°$, Fig. 12. In this case, the amplitude vector, after suffering the two phase shifts of 120° (Fig. 12a) again ends on the original (background) circle, but it is delayed somewhat in comparison to the background amplitude. The only contrast effect of the stacking fault under those conditions therefore would be to shift the thickness fringes in its area as projected on the image plane. Changing the sign of α_{in} (Fig. 12b) leads to a circle for the end points of the amplitude vector of the stacking fault which is distinctly different from the background circle and a good contrast is expected. This contrast behavior appears to be experimentally confirmed by the micrographs shown in Fig. 3 (in this case D_1 was approximately 37°; i.e. almost within the zero contrast region) and in Fig. 6, 7, and 8.

5. Discussion

It has been shown in the preceding section that if more than one phase shift is introduced along the path of the electron beams, i.e. if an extrinsic stacking fault, overlapping stacking faults or twin boundaries are present, a general asymmetry in the contrast can result when the sign of $(\boldsymbol{g} \cdot \boldsymbol{R}) \cdot s$ is changed if the distance between the planes of successive phase-shifts is larger than a few percent of the extinction distance.

This contrast effect is neither limited to weak-beam diffraction conditions nor to silicon or germanium as specimens, but should always occur if the above conditions are met. In particular, overlapping faults imaged with strong-beam conditions should show a contrast asymmetry if they are either rather widely spaced or very steeply inclined so that d_n becomes very large. Contrast asymmetries of overlapping stacking faults have indeed been observed (Fig. 9), consequently great care has to be taken as to the sign of α_{in} if real micrographs are to be compared to computed ones, as, e.g., in [4].

Quite dramatic contrast changes are predicted and have been observed, especially the disappearance of the fault contrast under certain conditions. The simple theory presented in the preceding section however cannot account for all the observed phenomena. Major difficulties which remain to be solved are

(i) the absence of contrast asymmetries in cases where it might be expected, e.g. for the extrinsic fault in Fig. 4 imaged with a {111} diffraction vector,

(ii) the contrast asymmetry with respect to the sign of $\boldsymbol{g}$ which may be concluded for intrinsic stacking faults from Fig. 5.

The striking absence of any detectable contrast asymmetry in the case of the extrinsic stacking faults imaged with an {111} diffraction vector (Fig. 4) might be due to shortcomings of the simple theory presented in this paper. These are neglect of segregation effects, i.e., concentration of impurity atoms at the stacking fault which may modify the local atomic scattering factors; break-down of the column approximation for steeply inclined stacked faults, and the assumption that the phase shift of the electron waves between the two faulted layers of an extrinsic stacking fault can be represented by the second integral in (3); i.e. in a continuum approximation. For a more accurate calculation this integral should be replaced by a summation over all the atoms between the faulted layers which would automatically take into account possible effects of higher order Laue zones (HOLZ). This could well lead to a total phase shift D_n substantially different from that derived here using the integral expression and also to differences between different diffraction vectors. Multi-beam effects might also influence the contrast and give rise to contrasts different for different kinds of diffraction vectors. Multi-beam effects have been shown, indeed, to produce contrast asymmetries at high accelerating voltages (600 kV) for intrinsic and extrinsic stacking faults [18].

The contrast asymmetries for intrinsic faults cannot be explained by the possible effects of HOLZ contributions or multi-beam effects. More involved dynamical multi-beam calculations [19] indeed do not predict any asymmetries. In principle an asymmetry of the contrast of intrinsic faults lying inclined to the image plane is expected if the finite Bragg angle is taken into account appropriately, i.e., if the column approximation is avoided. Such an asymmetry is due to the inherent asymmetry in the diffraction condition as illustrated in Fig. 13. However, corresponding contrast cal-

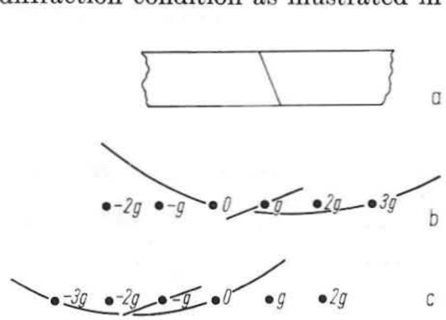

Fig. 13. Ewald sphere construction showing the inherent asymmetry in diffraction conditions upon reversing the sign of $\boldsymbol{g}$; a) position of the stacking fault in the foil, b) construction for $\boldsymbol{g}/3\boldsymbol{g}$ conditions, c) construction for $-\boldsymbol{g}/-3\boldsymbol{g}$ conditions. The Ewald sphere cuts the spike in reciprocal lattice caused by the stacking fault in different positions

culations (Wilkens unpublished) have shown that this effect gives contrast asymmetries of the order of, or less than, 1% under the image conditions applied in this paper. Another possibility is that a stacking fault is not adequately described by a translation vector $(a/6)\langle 112\rangle$ but that a small component perpendicular to the fault might be present, which either may be due to the presence of impurities in the fault [20] or may be an intrinsic property of stacking faults [21, 22]. Within the framework of two-beam theory this would not lead to a contrast asymmetry since α_{in} only changes in sign, but not in magnitude (which no longer would be 120°) with a sign change of $\boldsymbol{g}$. Multi-beam effects however may introduce an asymmetry in this case.

A situation similar to an intrinsic fault is the case of "special" grain boundaries (so-called coincidence or near-coincidence boundaries [23]) if they are imaged with a diffraction vector which is common to both crystals. In this case a rigid-body translation [9] (which may have several, symmetry related values) is thought to be present in the plane of the boundary [9]. The electron beams thus would suffer a phase shift related to the magnitude of the rigid-body translation vector. The boundary is therefore visible if imaged with a diffraction vector common to both crystals and exhibits a contrast very similar to that of an intrinsic stacking fault. Boundaries showing this particular behavior have been observed [8, 9] and it has been demonstrated that using weak-beam conditions they show a large contrast asymmetry if the sign of the diffraction vector is changed [8]. This is, as in the case of an intrinsic stacking fault, not in accordance with the theory presented. However, in this special case it is possible that the rigid-body translation is not entirely located at the interface but rather spread out over several lattice planes, i.e. the lattice planes perpendicular to the boundary are bent. Such an effect may occur in relatively low stacking fault energy materials as, e.g., silicon and stainless steel. It would introduce a fundamental asymmetry and could very well explain the contrast asymmetries in this case.

A similar explanation for intrinsic stacking faults seems to be less likely since any "spreading" of the translation vector would destroy the three-fold symmetry in the stacking fault plane.

Despite the serious problem which still remain to be solved, it is clear that great care has to be taken in the interpretation of weak-beam images of planar defects. Moreover, even conventional strong-beam images are not always free of contrast asymmetries and the detailed structure of planar defects as well as a proper consideration of the sign of $(\boldsymbol{g} \cdot \boldsymbol{R}) \cdot s$ has to be taken into account if erroneous conclusions are to be avoided.

Acknowledgements

The authors acknowledge discussions with Dr. W. A. T. Clark, Dr. J. M. Gibson, Dr. P. Fejes, Dr. I. P. Jones, Dr. M. H. Loretto, Dr. R. C. Pond, Dr. J. Silcox, Dr. J. C. H. Spence, Dr. V. Vitek, and Mr. A. P. Sutton. This work was partially supported by the National Science Foundation through the Materials Science Center at Cornell University.

References

[1] P. Hirsch, A. Howie, R. B. Nicholson, D. W. Pashley, and M. J. Whelan, Electron Microscopy of Thin Crystals, Butterworths, London 1965.

[2] S. Amelinckx, The Direct Observation of Dislocations, Academic Press, New York/London 1964.

[3] J. W. Edington, Practical Electron Microscopy in Materials Science, Van Nostrand Co., New York 1976.

[4] A. K. HEAD, P. HUMBLE, L. M. CLAREBROUGH, A. J. MORTON, and C. T. FORWOOD, Computed Electron Micrographs and Defect Identification, North-Holland Publ. Co., 1973.
[5] D. J. H. COCKAYNE, I. L.F. RAY, and M. J. WHELAN, Phil. Mag. **20**, 1265 (1969).
[6] A. G. CULLIS and G. R. BOOKER, Proc. 5th Europ. Congr. Electron Microscopy, Manchester 1972 (p. 532).
[7] C. A. FERREIRA LIMA and A. HOWIE, Phil. Mag. **34**, 1057 (1976).
[8] C. B. CARTER and H. FÖLL, Scripta metall. **12**, 1135 (1978).
[9] R. C. POND and V. VITEK, Proc. Roy. Soc. **A357**, 433 (1977).
[10] H. FÖLL, C. B. CARTER, and M. WILKENS, Proc. 37th Ann. EMSA Meeting, San Antonio (Texas) 1979 (p. 686).
[11] K. V. RAVI, Thin Solid Films **31**, 171 (1976).
[12] E. SIRTL and A. ADLER, Z. Metallk. **52**, 529 (1961).
[13] H. FÖLL and B. O. KOLBESEN, Semiconductor Silicon 1977, Ed. H. R. HUPP and E. SIRTL, Electrochemical Soc., Princeton (New Jersey) 1977 (p. 740).
[14] J. C. H. SPENCE, M. A. O'KEEFE, and H. KOLAR, Optik **49**, 307 (1977).
[15] J. DESSEAUX, A. RENAULT, and A. BOURRET, Phil. Mag. **35**, 357 (1977).
[16] R. C. POND, A. P. SUTTON, C. B. CARTER, and W. A. T. CLARK, Inst. Phys. Conf. Ser. No. 36 EMAG77, Glasgow 1977 (p. 247).
[17] H. FÖLL and B. O. KOLBESEN, to be published.
[18] L. J. CHEN and G. THOMAS, phys. stat. sol. (a) **25**, 193 (1974).
[19] D. K. SALDIN, private communication.
[20] O. L. KRIVANEK and D. M. MAHER, Proc. 35th Ann. EMSA Meeting, Boston (Mass.) 1977 (p. 20).
[21] I. P. JONES and H. L. LORETTO, Proc. 6th Europ. Congr. Electron Microscopy, Jerusalem 1976 (p. 503).
[22] J. B. WARREN and J. J. HREN, Proc. 34th Ann. EMSA Meeting, Miami Beach (Florida) 1976 (p. 488).
[23] W. BOLLMAN, Crystal Defects and Crystalline Interfaces, Springer-Verlag, Berlin 1970.

(Received January 23, 1980)